Materials Today Communications 32 (2022) 104101

Contents lists available at ScienceDirect

Materials Today Communications

journal homepage: www.elsevier.com/locate/mtcomm

Characterisation of polycaprolactone scaffolds made by melt electrospinning writing for pelvic organ prolapse correction - a pilot study

R. Rynkevic [a], M.E.T. Silva [a,*], P. Martins [a,b], T. Mascarenhas [c], J.L. Alves [a], A.A. Fernandes [a]

[a] LAETA, INEGI, Faculty of Engineering, University of Porto, Porto, Portugal
[b] ARAID, i3A, University of Zaragoza, Zaragoza, Spain
[c] Dep. of Obstetrics and Gynecology, CHSJ-EPE / Faculty of Medicine, University of Porto, Porto, Portugal

ARTICLE INFO

Keywords:
Biodegradable implants
PCL
Melt electrospinning technology
Prolapse repair
Mesh geometry
Degradation analysis
Additive manufacturing

ABSTRACT

Additive manufacturing and 3D printing technologies enable personalised treatments using custom-made prosthetics, implants and other medical devices. This research aimed to characterise novel biodegradable polycaprolactone (PCL) implants for pelvic organ prolapse repair, produced using melt electrospinning technology.

PCL mesh filaments were printed in 5 configurations: 240 μm, 160 μm, three layers of 80 μm, two layers of 80 μm and one layer of 80 μm. Material sterilisation, degradation, mechanical behaviour, and geometric variation due to applied loads were studied. Polypropylene (PP) Restorelle mesh was used as a reference in this study and vaginal tissue as a baseline.

Sterilisation by UV irradiation+ EtOH 70% did not affect the specimens. A significant weight loss was observed in 80 μm deposited fibers at 90 - and 180 - days of degradation, losing 10% of weight in neutral solution to 27% in acidic. All printed PCL deposited fibers had functional loss at 180 - day degradation in acidic solution (pH 4.2) ($p < 0.05$). PCL printed meshes were classified as ultra-lightweight, except lightweight 240 μm filament mesh. PCL meshes closely match the biomechanical properties of vaginal tissues, particularly in the comfort zone, unlike the Restorelle implant. The 3D printed mesh pores appeared to be stable compared to those of Restorelle meshes that had been used clinically until the FDA pulled its approval.

Based on the pilot study results, improved implant designs will be studied, and in vitro experiments on the cell adhesion and growth response will be conducted.

1. Introduction

Almost all commercially available surgical meshes for pelvic organ prolapse (POP) repair are knitted, consisting of continuous filaments (mono- or multifilament) and manufactured from four main polymers: polypropylene (PP), polyethene terephthalate (PET), polytetrafluoroethylene (PTFE), and polyvinylidene fluoride (PVDF) [1,2]. Many new implants have been introduced in the market without robust preclinical data [3]. Research in the area has expanded due to the vast number of post-surgery complications such as infection, fibrosis, adhesions, mesh rejection, and prolapse recurrence [3]. Insufficient biocompatibility and inappropriate biomechanical properties of the implants, combined with patient and surgeon factors, might be the reason for local complications [3]. Lighter weight, larger pore size, monofilament meshes are thought to be associated with better host tolerance and lower complication rates [4]. According to the above concepts, one of the latest clinical implants, Restorelle mesh (Coloplast, Humlebaek, Denmark) had theoretically advantageous properties [5]. However, the Food and Drug Administration (FDA) ordered Coloplast to immediately stop selling and distributing these products because "reasonable confidence in the safety and effectiveness of these devices" used to treat POP has not been demonstrated since the agency categorized them as high risk in 2016 [6]. One possible explanation for graft related complications (GRCs) could be the persistent inflammatory response induced by durable materials [7]. Therefore, degradable scaffolds may be more adequate. Pore stability also plays an essential role in tissue ingrowth. The original pore size can be reduced when loaded (pores "collapse"), preventing proper tissue ingrowth [8].

Today, personalised medicine considers the individual differences among patients and uses them to find the proper treatment, promptly.

* Correspondence to: LAETA, INEGI, Faculty of Engineering, University of Porto, Rua Dr. Roberto Frias s/n, 4200-465 Porto, Portugal.
E-mail addresses: r.rynkevic@gmail.com (R. Rynkevic), mesilva@inegi.up.pt (M.E.T. Silva), pedro.sousamartins@gmail.com (P. Martins), tqc@sapo.pt (T. Mascarenhas), falves@fe.up.pt (J.L. Alves), aaf@gcloud.fe.up.pt (A.A. Fernandes).

https://doi.org/10.1016/j.mtcomm.2022.104101
Received 22 January 2022; Received in revised form 22 July 2022; Accepted 25 July 2022
Available online 26 July 2022

Researchers have dedicated significant effort to address these problems in investigating tissue regeneration approaches. One of the technologies that enable tailor-made treatments is additive manufacturing with 3D printing technologies already used to create custom-made prosthetics, implants and other medical devices [9]. Melt electrospinning writing (MEW) is a fibre-based manufacturing technique used to design and build scaffolds with sufficient mechanical strength [10]. The flexibility of 3D printing allows the creation of medical devices with very complex internal structures, matching a patient's anatomy [11]. The possibility to mimic the features of biological tissues, with complex hierarchical structures, without compromising cellular proliferation, growth and angiogenesis (responsible for forming and remodelling the vascular network) is essential in tissue engineering applications [12,13]. Moreover, the main advantage of melt electrospinning technology is the possibility of fabrication of ultrafine polymer fibres without solvents, avoiding toxicity issues [14].

This research was focused on the mechanical characterisation, in vitro degradation studies and geometric variation analysis of biodegradable polycaprolactone (PCL) novel implants for POP repair produced using MEW technology. Geometric parameters have been recreated using a recent clinical implant Restorelle mesh for comparison purposes, used as a reference in this study [5].

2. Materials and methods

2.1. Materials and 3D printing

Biodegradable PCL, used in this research, has been approved for use in humans by the FDA [15]. PCL is a material widely used in electrospinning processes [16]. The filament used is a commercially available (non-medical grade) variant sold by 3D4Makers, named Facilan™ PCL 100, with density 1.1 g/cm (ISO 1183), filament diameter 1.75 mm, glass transition temperature − 60 ºC, melting point 58–60 ºC, decomposition temperature 200 ºC, and melt flow index 11.3–5.2 g/10 min

The MEW prototype "SPINMESH" machine was used to produce novel PCL meshes [10]. The device was built using an XY moving collecting plate and a Z moving printing head on an aluminium box structure. The positive high voltage was applied to the collector and the negative was connected to the nozzle.

2.2. In vitro studies: material sterilisation and degradation analysis

For in vitro degradation studies, 3D printed fibers used to create implants was a minimalised final mesh model. PCL fibers were printed at 200 ºC temperature, using 2750 mm/min linear speed and 6.5 kV voltage in 5 configurations: one layer of 240 μm, one layer of 160 μm, three layers of 80 μm, two layers of 80 μm and one layer of 80 μm. Six 80 mm length samples were prepared for each group. In the work reported the temperature was measured on the nozzle and not in the PCL extrusion melt.

In this study the equipment's parameters were the same as those presented by Cunha et al. [10], considering the accurate result (minimum error). To print different diameters, we only changed the extrusion rate (E) according to Eq. 1.

$$E = L_{out}\frac{d_{out}^2}{1.75^2} \quad (1)$$

Where L_{out} is the printed fiber length, d_{out} is the diameter (80 μm, 160 μm and 240 μm), and 1.75 is the PCL filament diameter".

PCL filaments were sterilized via exposure to UV light irradiation (254 nm) for 30 min per side, followed by incubation in ethanol EtOH 70% for 1 h. Then, samples were rinsed using with Phosphate Buffer Solution (PBS) 2 times over 30 min, and dried within the flow chamber prior to use. Fibers were weighed before and after sterilization and were tested under the uniaxial tensile loading to evaluate effects of sterilization on mechanical behaviour.

The in vitro biodegradation test of material due to exposure to the biological environment was carried out in compliance with the standard ISO 10993 "Biological evaluation of medical devices" [17]. PBS was used as a model of biological fluid, to study the processes of dissolution and resorption in vitro [18,19]. One tablet was dissolved in 200 mL of distilled water to obtain a solution with pH = 7.4. The biodegradation can occur under a wide range of pH, including acid mediums associated with inflammation [20]. Therefore, Potassium Hydrogen Phthalate (KHP) [18,21] was used to obtain the acid medium. One tablet was dissolved in 100 mL of distilled water to obtain a solution of pH = 4.3. Each specimen's thickness and initial weight were measured before immersion into KHP and PBS solutions. Analytical balance with an inherent error of ± 0.0001 g for each reading was used. An automatic pH meter was used to control the acidity index in the tube. Samples were kept at 37 °C (± 0.1 ºC) during 7, 30, 42, 60, 90 and 180 days, repeating established protocol time points used in previous animal studies [22–24]. After the degradation process, the samples were washed in distilled water, dried at room temperature for 24 h and weighed. The degradation of the material was evaluated via weight loss. Dried samples were subjected to uniaxial mechanical testing to evaluate their functional loss and scanning electron microscope (SEM) analysis to evaluate filament surface corrosion.

2.3. 3D Mesh printing and characterisation

The geometry of novel 3D printed PCL meshes was reproduced and benchmarked with a commercially available Restorelle mesh. The Restorelle is a lightweight polypropylene (PP) mesh with a density of 19 g/m^2, composed of three knitted monofilaments (80 μm diameter) with a 1.6 − 2.0 mm pore size. The prototype PCL meshes produced by MEW were printed in five configurations (Fig. 7), mimicking simple square-shaped geometrical pattern and pore size of Restorelle. The variation parameters were fiber diameter and number of layers. One layer meshes with 240 μm, 160 μm and 80 μm fiber diameters, and two and three layers meshes with 80 μm fibers diameter were produced. Printed PCL meshes samples (80 ×80 mm) were weighed using an analytical balance, with an inherent error of ± 0.001 g for each reading, to calculate the density.

Novel printed meshes were cut out into 60 × 10 mm strips, respecting the pore pattern (10 mm from each size for specimen fixation). These sample dimensions were chosen to allow a constant length-to-width aspect ratio of 4 to minimise the nonlinear effects of clamping on the uniaxial mechanical properties. A total of four specimens were obtained for each mesh and analysed via mechanical testing, image analysis and SEM.

2.4. Uniaxial testing protocol and pore deformation analysis

As a first step into the pipeline to clinical assessment [25], the material properties are obtained via mechanical testing. Tensile testing is generally acknowledged as the primary method to study the material's properties and is often used to predict the behaviour of a material under more complex loading conditions.

An electronic testing machine, "Mecmesin Multi test 2.5" was used to conduct the tensile tests on the produced meshes using a 100 N load cell (Mecmesin AFG 100 N). A preload of 0.1 N was applied to remove all slack from the mesh. This point was defined as elongation zero. A constant elongation rate of 10 mm/min was then used to load the specimen until failure. Outcome measurements describing the mechanical properties of PCL fibers and meshes were stress-strain curves. Vaginal tissue mechanical behaviour was obtained from previous studies and was used as a baseline [25]. The toe region of the stress-strain curve (comfort zone) is usually considered to be within the physiological range of deformation. Meanwhile, the linear part of the stress-strain curve is in the range of supra-physiological stress (stress zone). The stress

Table 1
Fibers weight loss (%) after sterilization and degradation. The significant difference noted when $p < 0.05$ (*).

Sterilisation	Fiber weight loss after sterilization (%)									
	240 μm		160 μm		80 μm (3 layers)		80 μm (2 layers)		80 μm (1 layer)	
	0.43		0.62		0.34		0.17		3.75	
Degradation time point	**Fiber weight loss after degradation (%)**									
	240 μm		**160 μm**		**80 μm (3 layers)**		**80 μm (2 layers)**		**80 μm (1 layer)**	
	PBS	**KHP**	**PBS**	**KHP**	**PBS**	**KHP**	**PBS**	**KHP**	**PBS**	**KHP**
7d	0	0	0	0	0	0	0	0	0	0
30d	0.38	0.77	0.97	1.57	1.17	1.18	1.69	1.72	3.46	4.01
42d	0.38	0.77	0.94	1.81	1.16	3.41	3.17	3.64	3.56	4.83
60d	0.41	0.87	1.83	2.39	2.27	3.53	3.33	3.75	3.71	7.61
90d	0.93	1.15	2.75	3.45	2.59	3.95	3.63	5.26	10.3 *	11.53 *
180d	1.20	1.96	3.18	3.68	4.11	5.43	8.33 *	10.17 *	14.28 *	27.57 *

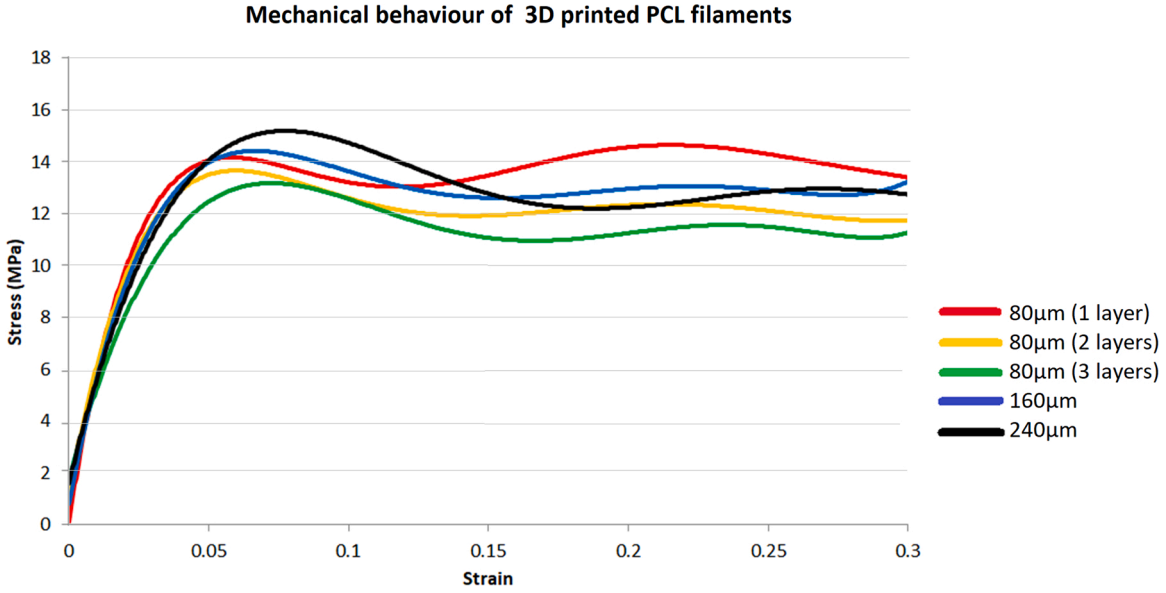

Fig. 1. Stress–strain curve showing typical yield behaviour of polycaprolactone fibers, during uniaxial tensile loading.

estimation value is a nominal value calculated using as cross section of the specimen: width of the specimen (10 mm) x an equivalent thickness equal to the deposited fibers diameter (240 μm, 160 μm and 80 μm).

Digital camera records during the tensile testing were used to analyse mesh pore deformation. Images were captured at each millimetre of mesh elongation during tensile testing. Images were processed using ImageJ software [26], and overall geometric variations during tensile loading (length, width and area) were analysed.

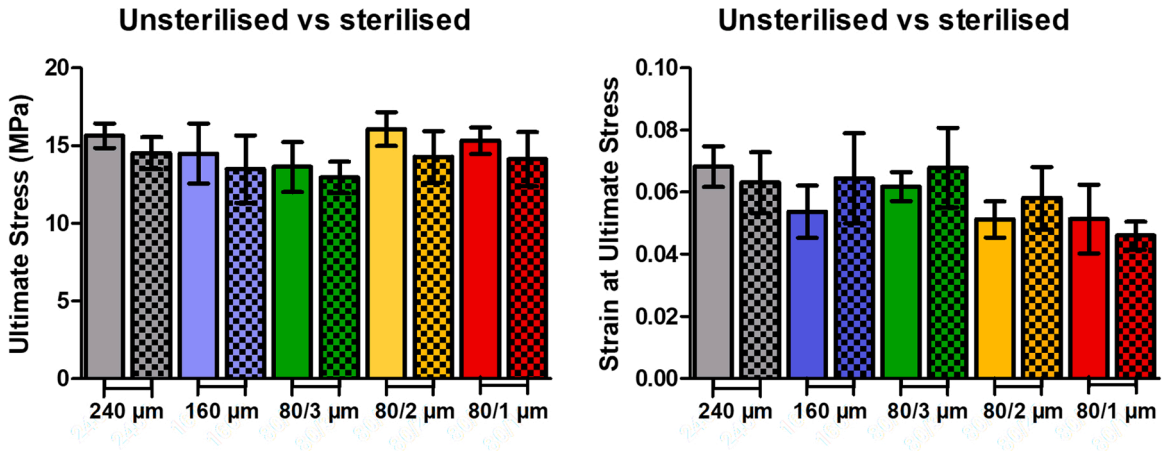

Fig. 2. Vertical column bar graphs (mean with ± SD), representing comparative analysis stress and strain parameters of different deposited fibers before and after sterilisation. The colour coding of the fibers was chosen according to Fig. 1; unsterilized fibers (solid bars), sterilised fibers (chess bars). The significant difference noted when $p < 0.05$ (*).

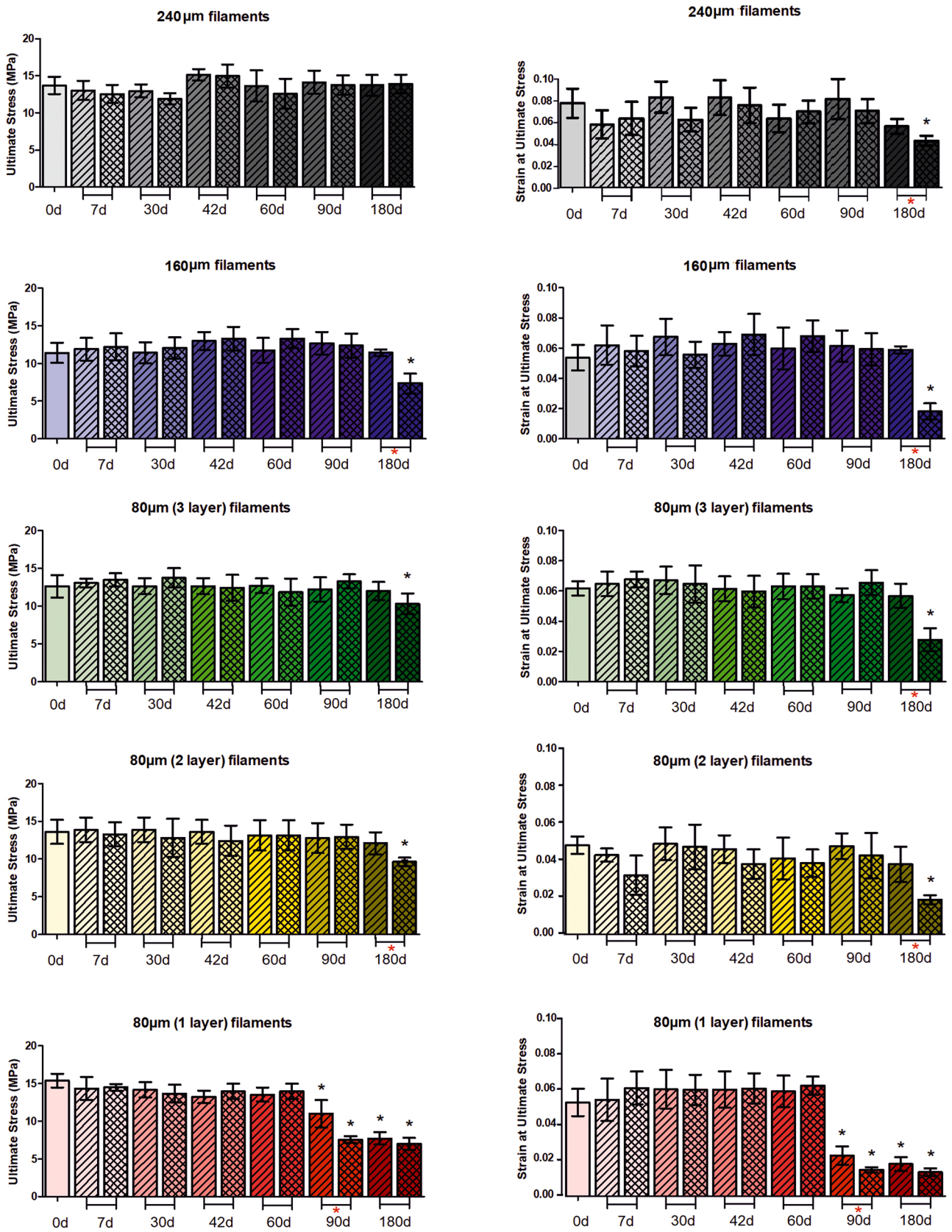

Fig. 3. Vertical column bar graphs (mean with ± SD), representing comparative analysis stress and strain parameters of different fibers before and after in vitro degradation test. The colour coding of the groups was chosen according to Fig. 1; dry fibers (solid bars), fibers after degradation in PBS (diagonal line bars), fibers after degradation in KHP (crossed bars). The significant difference noted when $p < 0.05$ (*): Dry vs degraded are indicated under the bars (*), intergroup comparison (acidic and neutral environment) is displayed below the bars (*).

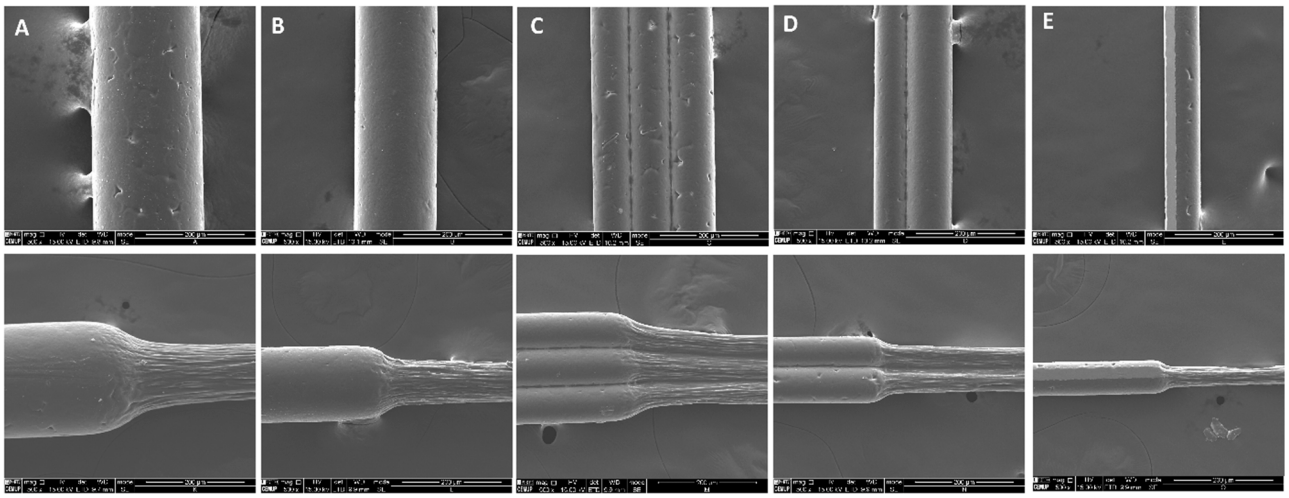

Fig. 4. SEM images of PCL fibres (A - 240 μm; B - 160 μm; C - 80 μm/ 3 layers; D - 80 μm/ 2 layers; E - 80 μm/ 1 layer) produced by melt electrospinning (500 x magnification): Top row – novel printed fiber; Bottom row – degraded and tensioned fibers. Scale: 2 mm.

2.5. Scanning Electron Microscopy (SEM) analysis

The fibers surface corrosion, induced during degradation experiments and mesh structure (pore size collapse and bundling effect), after uniaxial tensile tests, was studied using a SEM analysis. It was performed using a high resolution (Schottky) Environmental Scanning Electron Microscope with X-ray microanalysis and electron backscattered diffraction analysis: FEI Quanta 400 FEG ESEM / EDAX Genesis X4M. All the samples were coated with an Au/Pd thin film, by sputtering, for 80 s

2.6. Statistical analysis

Statistics were done using GraphPad Prism 5 (GraphPad Software, Inc., La Jolla, CA, USA). The normality of the data was verified using the Kolmogorov-Smirnov test. Quantitative data are reported as mean ± standard deviation (SD). One-way ANOVA analysis and Dunnett's post-test correction was used to determine whether the differences between multiple pairs were statistically significant. The level of significance was set to $p < 0.05$. Unpaired Student's t-test analysed the sterilisation effect (confidence level of 95%, level of significance $p < 0.05$).

3. Results

3.1. PCL printed fibers analysis

Weight loss was present in the specimens after selected sterilization (UV irradiation + EtOH 70%), but it was not significant (Table 1). A significant weight loss was observed in 80 μm fiber on the 90-th and 180-th day of degradation in both media, losing approximately 10–27% of the weight (Table 1). 2-layered 80 μm fibers also significantly lost weight on the 180-th day of degradation, by 8.33% in buffer solution and 10.17% in acidic solution. No significant weight loss was found among the other fibers; however, its pattern due to degradation was noticed. The longer the degradation is, the more weight is lost, mainly in the acidic environment.

Despite the different printing configurations, all printed fiberss have identical behaviour under tensile stress. Stress, exceeding the 13–14 MPa yield strength, led to plastic deformation (Fig. 1). In sterilized samples, a decrease in ultimate stress (by 7–8%) was observed, but changes in mechanical behaviour were not significant; ultimate stress values were within statistical error (Fig. 2). After 180-day degradation in acidic media, all printed fibers became more fragile and with maximum strain reduced to half ($p < 0.05$) (Fig. 3). The thinnest 80 μm fibers had a significant mechanical strength and functional loss in both media at 90- and 180- days degradation ($p < 0.05$).

SEM images of PCL electrospun printed fibers are displayed in Fig. 4. It is possible to see some imperfections due to printing. No specific changes on the fiber surface after sterilization and degradation were observed. Fibre remained uniform and solid. Tensioned fibers were not breaking yet stretching (yielding).

Table 2
Mesh classification based on the weight (lightweight (35–69 g/m^2), ultra-lightweight (<35 g/m^2)) [26].

Mesh type	Density (g/m^2)	Classification
PP (Restorelle)	19.00	ultra-lightweight
PCL (240 μm)	48.70	lightweight
PCL (160 μm)	24.00	ultra-lightweight
PCL (80 μm/ 3 layers)	27.73	ultra-lightweight
PCL (80 μm/ 2 layers)	18.83	ultra-lightweight
PCL (80 μm/ 1 layer)	9.58	ultra-lightweight

3.2. 3D printed PCL mesh characterisation

In Table 2, printed PCL meshes are presented based on their density, and classified as suggested by Cobb et al. [22]. All meshes except PCL (240 μm) were classified as ultra-lightweight (< 35 g/m^2). According to this grading system, PCL (240 μm) was a lightweight mesh (35–69 g/m^2). In contrast, the lowest density of 9.58 g/m^2 was observed in PCL (80 μm/ 1 layer). Closest to the Restorelle mesh was PCL (80 μm/ 2 layers), with a density of 18.83 g/m^2.

Printed PCL meshes mechanical behaviour during tensile testing was compared to vaginal tissue mechanical behaviour from a healthy sheep [25] and PP Restorelle mesh (Fig. 5A). The mesh prototype's behaviour was distinct from the behaviour of both the commercial product and the vaginal tissue. However, considering the comfort zone (physiological range of deformation), the one-layer PCL mesh with a fibre diameter of 80 μm matched the tissue properties (Fig. 5B). Restorelle mesh was significantly stiffer than vaginal tissue ($p < 0.05$).

Restorelle mesh underwent various geometric transformations during a uniaxial tensile test (Fig. 6A). At the beginning of the deformation, the Restorelle specimen area increased by 10% and then decreased by 17.5%. All 3D printed PCL meshes areas increased linearly during uniaxial loading by 12–20% (Fig. 6B). Restorelle mesh width decreased linearly by 25%, creating an hourglass effect, while PCL meshes width appears to be stable, decreasing linearly by 1–4.5%. In Restorelle, pore

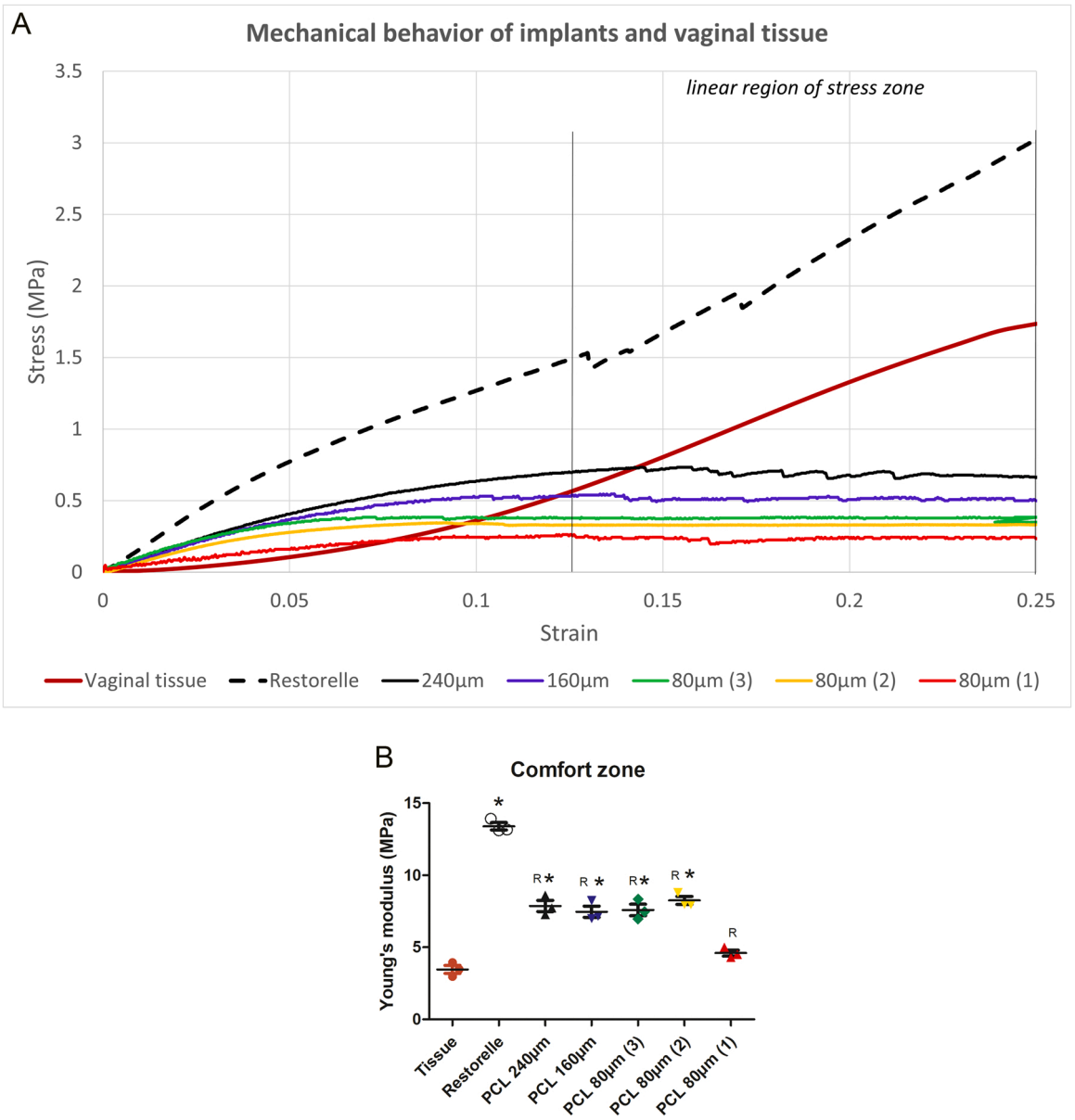

Fig. 5. A- Mechanical behaviour of five variants of 3D printed PCL meshes during uniaxial tensile testing, compared with vaginal tissue and Restorelle mesh. B- Vertical scatter plot, mean with ± SD of Young's modulus at comfort zone. Significant differences among meshes and vaginal tissue (*) marked as (*), the difference with Restorelle marked as (R). Significant difference noted when $p < 0.05$.

axial deformation and narrowing occurring along the entire specimen is clearly visible, whereas PCL mesh pores seem steady. Only in areas where the yield point was achieved, the pores were deformed, increasing the area. However, the yield stress took place outside the so-called comfort zone.

Plastic deformation occurred in all mesh specimens (Fig. 7). Restorelle mesh pores were breaking, and a narrowing effect (collapse) was observed, while PCL printed meshes pores were not breaking yet stretching (yielding).

4. Discussion

This research had as its main aim the development and characterization of novel PCL biodegradable 3D printed meshes for POP repair that mimics the physiologic biomechanics of the vaginal wall. A complex analysis and characterization of the electrospun material's mechanical behaviour and degradation and mesh design, was carried out.

Controlled in vitro degradation analysis was carried out, to study the material design and fabrication factors that might affect in vivo tissue integration [27]. The working life of biodegradable medical devices has two stages: the first is functional, when the implant performs tissue function, and the second is passive when the native tissue gradually replaces the implant. However, the biodegradation process might alter the host inflammatory response, creating an unfavourable environment, characterized by a local acid pH, that could lead to premature loss of functional properties of the implant [20]. This means, that the material degradation rate should not exceed the recovery rate. Over time, the PCL filaments did not demonstrate significant weight loss; only at 180 days, 160 µm filaments (2 fibers with 80 µm diameter) and 80 µm filament significantly lost their weight. For the acidic solution (pH 4.2), all printed PCL filaments had functional loss at 180-day degradation. Comparing our previous experimental studies with new data, we can say that in the early stages of mesh implantation, even with an inflammatory reaction, the functional life of the implants will not change [22]; in the later stages, tissue regeneration is already in progress [24]. It was observed that the degradation and sterilization did not cause significant

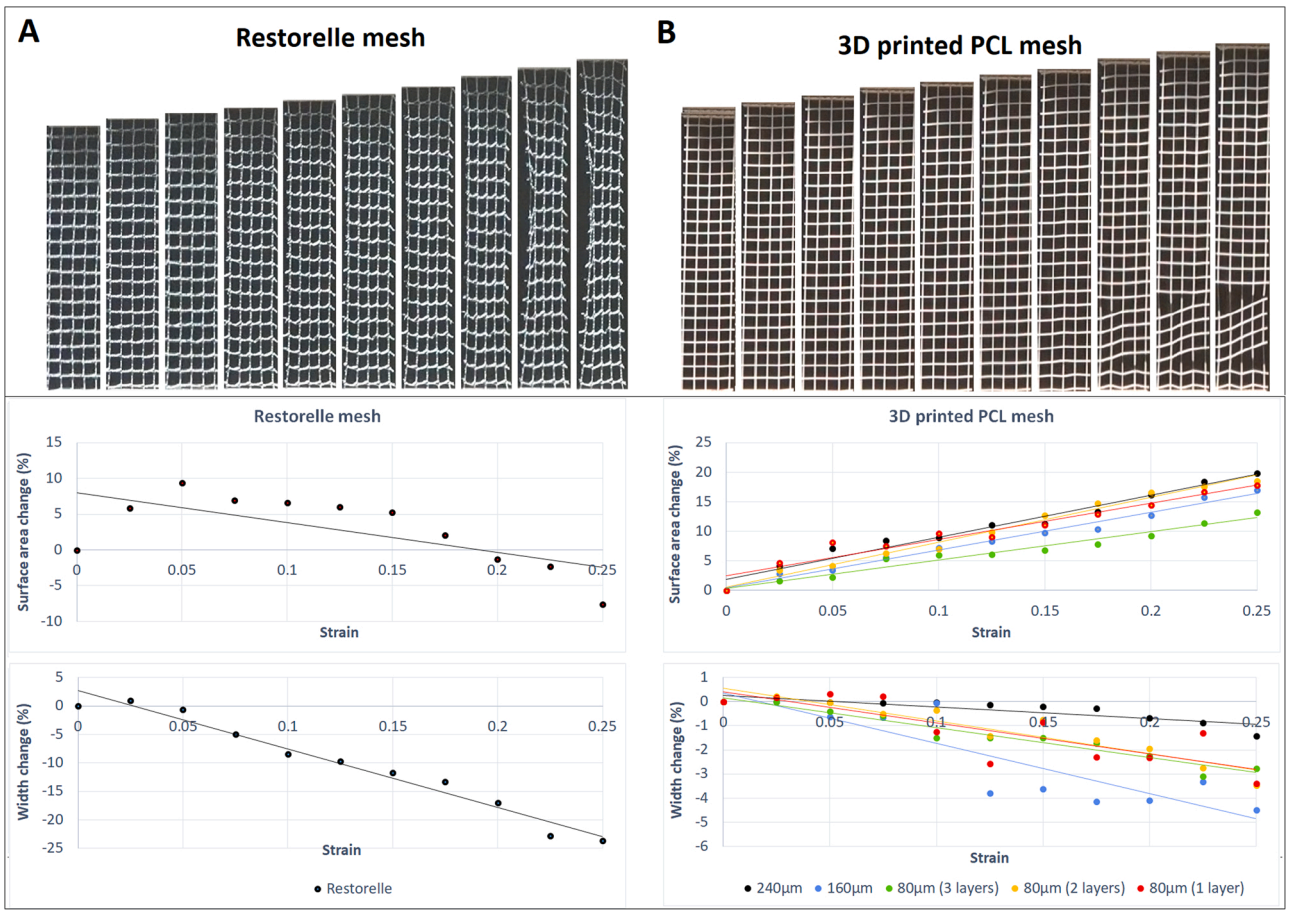

Fig. 6. A - Restorelle mesh, B - 3D printed PCL mesh. Images above - mesh geometric changes during a uniaxial tensile test, depicted at every millimetre of deformation. Graphs below - mesh area variation (%) and width changes (%) during a uniaxial tensile test.

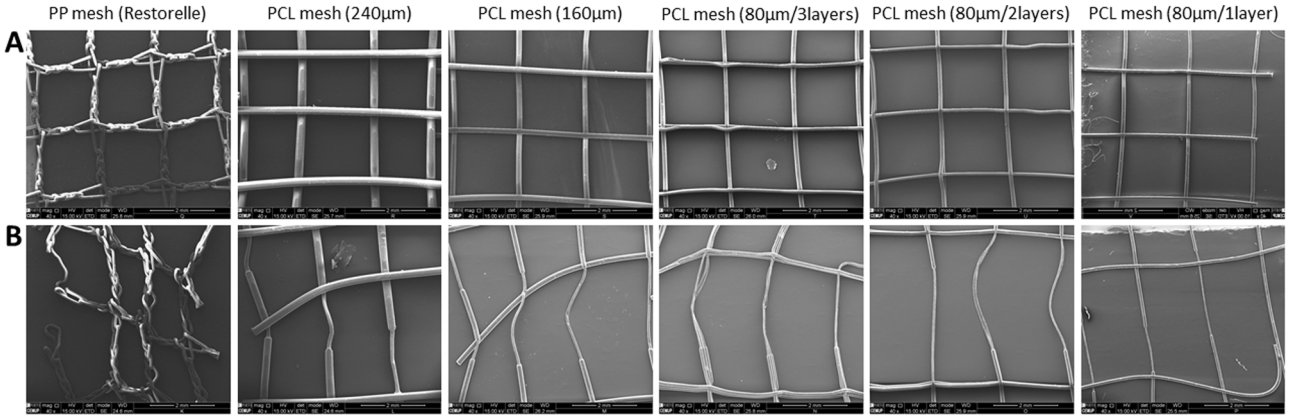

Fig. 7. SEM images of the meshes before and after uniaxial tensile test: A - initial state, B - afterload condition. Scale: 2 mm (bottom right).

surface changes on the printed filaments.

All mesh configurations were used to develop implants for POP repair; the mesh geometry selected was similar to a commercially available polypropelene mesh, Restorelle, for benchmarking purposes. Implant weight and density may also affect the host response [28]. Cobb et al. classified meshes based on their weight: heavy weight (> 140 g/m^2), mid-weight (70–139 g/m^2), lightweight (35–69 g/m^2) and more recently, ultra-lightweight meshes (< 35 g/m^2) [26]. All printed meshes were ultra-lightweight, except the 240 µm meshes, which were lightweight). Lightweight meshes may induce better physiological compliance of the host tissue, after ingrowth. This is due to a lower material burden in the host, reducing scar formation and preserving the elasticity of the tissue [28,29]. Ideally, meshes initial biomechanical properties should match those of the host tissue, yet with a structure that promotes tissue ingrowth. Post-surgical complications can also be related to pore size: when smaller than 1 mm, the risk of infection due to poor tissue ingrowth and fibrotic encapsulation, increases [2,30]. In a previous study, the surgeons suggest a mesh with large pores (>1 mm) avoid pore collapse [31]. Restorelle mesh and the PCL biodegradable printed meshes had a 1.8 and 2.0 mm pore size respectively, which are considered large pore size meshes, thus promoting better tissue ingrowth [32].

After implantation, the mesh becomes part of the muscle-fascial complex, and besides repairing the defect, should function together with the muscles and fascia [33]. This can induce complications, linked, among other causes, to mismatch of the mesh/tissue's mechanical properties under acting tensile loads [32]. One of the reasons might be mesh pore stability, which plays a vital role in tissue integration. When loaded, the initial pore size can be reduced due to pore "collapse", precluding proper tissue ingrowth [5]. Post-operative changes in pore dimensions of a textile implant, have been reported, when the implant undergoes immediate post-implantation deformation, that could also cause GRCs [34]. Mechanical testing may simulate immediate post-implantation deformation and the functional performance of the mesh; thus, post-operative geometrical changes and the clinically relevant failure mechanisms of implants can be evaluated. mechanical tests carried out with the Restorelle mesh showed mesh filament bundling with "out of plane deformation" and pore collapse, with mesh area reduction, which has been associated to the occurrence of associated GRC's, such as erosions [5]. It was observed that the printed meshes follow closely the biomechanical properties (stiffness) of vaginal tissues, unlike the polypropelene Restorelle implant, particularly in the comfort zone. In this region, the prototype 3D printed meshes support lower loads than the commercial mesh, but its mechanical behaviour is comparable to vaginal tissue. As illustrated in Fig. 5, at the end of the toe region of the comfort zone, elongation of the mesh, with plastic deformation and limited load is observed.

The flexibility of 3D printing allows quick changes to the mesh design, without additional equipment or tools. This technology may also be used by manufacturers to create implants with very complex internal structures, that match the patient's anatomy (patient-specific/personalized devices). The "SPINMESH" prototype, used in the present work, allows the use of materials in pellets or filament form. It is also possible to print simultaneously biodegradable and non-degradable polymers. The results reported were obtained with 3D printed biodegradable mesh prototypes. Research in progress will study new implant structures with functionally graded or partially graded options. It is planned also to perform experiments in vitro and *in with the novel meshes* to better understand the influence of the pore size and geometry of biodegradable mesh produced by melt electrospinning writing on host response.

5. Conclusions

In this study, prototype biodegradable meshes, mimicking the geometry of a commercially available mesh (Restorelle), for benchmark purposes, were manufactured, using melt electrospinning writing technology. The 3D printed biodegradable mesh's prototypes, showed mechanical properties (stiffness) closer to vaginal tissue properties than Restorelle (stiffer and stronger). Further, the 3D printed meshes displayed a more isotropic behaviour that the non-degradable polypropelene Restorelle mesh, which, when tensile loaded, show out of plane deformation with fiber bundling and pore collapse, causing graft related complications in particular mesh erosion. The results obtained so far with the 3D printed biodegradable meshes are very promising. Thus, it is expected that this research outcomes will contribute to the development of a new generation of meshes and new methodologies to obtain rigorous clinical data for premarket approval of the devices for prolapse repair, as currently required by the FDA, before being marketed as Class III devices (generally high-risk devices).

CRediT authorship contribution statement

All the authors have made substantial contributions to the production of the final manuscript, including the conception and design of the study, acquisition of data, analysis and interpretation of the obtained results, clinical evaluation of results, drafting the article and revising it. All the authors present in the article have approved the final version submitted. The manuscript submitted for publication, including related data and figures, has not been previously published and is not considered elsewhere.

Declaration of Competing Interest

The authors declare that they have no known competing financial interests or personal relationships that could have appeared to influence the work reported in this paper.

Data Availability

No data was used for the research described in the article.

Acknowledgments

The authors gratefully acknowledge the funding by Ministério da Ciência Tecnologia, e Ensino Superior, FCT - Fundação para a Ciência e a Tecnologia, Portugal and Programa Operacional Competitividade e Internacionalização - POCI the project SPINMESH - Melt electrospinning of polymeric bioabsorbable meshes for pelvic organ prolapse repair - POCI-01-0145-FEDER-029232. The authors would like to thank Eng. Andre Brandao and Eng. Andressa Belo for technical support in this research.

References

[1] S. Elango, S. Perumalsamy, K. Ramachandran, K. Vadodaria, Mesh materials and hernia repair, Biomedicine 7 (3) (2017) 16.
[2] Y. Bilsel, I. Abci, The search for ideal hernia repair; mesh materials and types, Int. J. Surg. 10 (6) (2012) 317–321.
[3] Food and Drug Administration, "Serious Complications Associated With Transvaginal Placement of Surgical Mesh in Repair of Pelvic Organ Prolapse and Stress Urinary Incontinence.,"," Food and Drug Administration FDA, Public Health Notification, 2008. ⟨http://www.amiform.com/web/documents-risques-op-coelio-vagi/fda-notification-about-vaginal-mesh.pdf⟩.
[4] L.M. Zhu, P. Schuster, U. Klinge, Mesh implants: an overview of crucial mesh parameters, World J. Gastrointest. Surg. 7 (10) (2015) 226–236.
[5] W.R. Barone, P.A. Moalli, S.D. Abramowitch, Textile properties of synthetic prolapse mesh in response to uniaxial loading, Am. J. Obstet. Gynecol. 215 (3) (2016) 1–9.
[6] U.S. Food and Drug Administration, "FDA takes action to protect women's health, orders manufacturers of surgical mesh intended for transvaginal repair of pelvic organ prolapse to stop selling all devices," U.S. Food and Drug Administration, 16 04 2019. [Online]. Available: ⟨https://www.fda.gov/news-events/press-announcements/fda-takes-action-protect-womens-health-orders-manufacturers-surgical-mesh-intended-transvaginal⟩. [Accessed 13 02 2021].
[7] J.M. Anderson, A. Rodriguez, D.T. Chang, Foreign body reaction to biomaterials, Semin Immunol. 20 (2) (2008) 86–100.
[8] S.P. Lake, S. Ray, A.M. Zihni, D.M. Thompson Jr., J. Gluckstein, C.R. Deeken, Pore size and pore shape–but not mesh density–alter the mechanical strength of tissue ingrowth and host tissue response to synthetic mesh materials in a porcine model of ventral hernia repair, J. Mech. Behav. Biomed. Mater. 42 (2015) 186–197.
[9] B.K. Gu, D.J. Choi, S.J. Park, et al., 3D bioprinting technologies for tissue engineering applications, Adv. Exp. Med. Biol. 1078 (2018) 15–28.
[10] Cunha M.N., Rynkevic R., Silva M.E.T., Brandão A., Alves J.L., Fernandes A.A., Melt Electrospinning Writing of Mesh Implants for Pelvic Organ Prolapse Repair., 3D Printing and Additive Manufacturing, 2021, Ahead of Print. Doi:10.1089/3dp.2021.0010.
[11] F.M. Wunner, S. Florczak, P. Mieszczanek, O. Bas, E.M. De-Juan-Pardo, D. W. Hutmacher, Electrospinning with polymer melts – state of the art and future perspectives, Compr. Biomater. II (2017) 217–235.
[12] I. Jun, H.S. Han, J.R. Edwards, H. Jeon, Electrospun fibrous scaffolds for tissue engineering: viewpoints on architecture and fabrication, Int. J. Mol. Sci. 19 (3) (2018) 745.
[13] J. Lannutti, D. Reneker, T. Ma, D. Tomasko, D. Farson, Electrospinning for tissue engineering scaffolds, Mater. Sci. Eng. C 27 (3) (2007) 504–509.
[14] A. Bachs-Herrera, O. Yousefzade, L.J. del Valle, J. Puiggali, Melt electrospinning of polymers: blends, nanocomposites, additives and applications, Appl. Sci. 11 (2021) 1808.
[15] R. Dwivedi, S. Kumar, R. Pandey, et al., Polycaprolactone as biomaterial for bone scaffolds: review of literature, J. Oral. Biol. Craniofac. Res. 10 (1) (2020) 381–388.
[16] M.P. Arrieta, A. Leonés Gil, M. Yusef, J.M. Kenny, L. Peponi, Electrospinning of PCL-Based Blends: Processing Optimization for Their Scalable Production, Materials 13 (17) (2020) 3853.
[17] 10993–2011, ISO, Estimation of biological activity of medical products, 2011.
[18] ISO 13781–2011, Resins and shaped elements poly-L-lactide for surgical implants. Degradation research in vitro, 2011. ⟨https://gostperevod.com/gost-r-iso-13781–2011.html⟩.

[19] Sigma-Aldrich. Phosphate buffered saline-Sigma-Aldrich Co. LLC. ⟨https://www.sigmaaldrich.com/catalog/product/sigma/p4417?lang=pt&region=PT⟩ Accessed 20 July 2022.
[20] P. Galgut, I. Waite, R. Smith, Tissue reaction to biodegradable and non-degradable membranes placed subcutaneously in rats, observed longitudinally over a period of 4 weeks, J. Oral. Rehabilit. 23 (1996) 17–21.
[21] Sigma-Aldrich. Potassium hydrogen phthalate. Sigma-Aldrich Co. LLC. ⟨https://www.sigmaaldrich.com/PT/en/substance/potassiumhydrogenphthalate20422877247⟩ Accessed 21 July 2022.
[22] L. Hympanova, M.G.M.C. Mori da Cunha, R. Rynkevic, M. Zündel, M.R. Gallego, J. Vange, G. Callewaert, I. Urbankova, F. Van der Aa, E. Mazza, J. Deprest, Physiologic musculofascial compliance following reinforcement with electrospun polycaprolactone-ureidopyrimidinone mesh in a rat model, J. Mech. Behav. Biomed. Mater. 74 (2017) 349–357.
[23] M.G.M.C.M. da Cunha, L. Hympanova, R. Rynkevic, T. Mes, A.W. Bosman, J. Deprest, Biomechanical behaviour and biocompatibility of ureidopyrimidinone-polycarbonate electrospun and polypropylene meshes in a hernia repair in rabbits", Materials 12 (7) (2019).
[24] L. Hympanova, M.G.M.C. Mori da Cunha, R. Rynkevic, R.A. Wach, A.K. Olejnik, P. Y.W. Dankers, J. Deprest, Experimental reconstruction of an abdominal wall defect with electrospun polycaprolactone-ureidopyrimidinone mesh conserves compliance yet may have insufficient strength, J. Mech. Behav. Biomed. Mater. 88 (2018) 431–441.
[25] K.A. Jones, A. Feola, L. Meyn, S.D. Abramowitch, P.A. Maolli, Tensile properties of commonly used prolapse meshes, Int. Urogynecol. J. 20 (2009) 847–853.
[26] W.S. Cobb, J.M. Burns, R.D. Peindl, A.M. Carbonell, B.D. Matthews, K.W. Kercher, B.T. Heniford, Textile analysis of heavy weight, mid-weight, and lightweight polypropylene mesh in a porcine ventral hernia model, J. Surg. Res. 136 (1) (2006) 1–7.
[27] B.A. Whitson, B.C. Cheng, K. Kokini, S.F. Badylak, U. Patel, R. Morff, C.R. O'Keefe, Multilaminate resorbable biomedical device under biaxial loading (Fall), J. Biomed. Mater. Res. 43 (3) (1998) 277–281, https://doi.org/10.1002/(sici)1097-4636(199823).
[28] J.M. Bellón, M. Rodríguez, N. García-Honduvilla, V. Gómez-Gil, G. Pascual, J. Buján, Comparing the behavior of different polypropylene meshes (heavy and lightweight) in an experimental model of ventral hernia repair, J. Biomed. Mater. Res. B Appl. Biomater. 89 (2) (2009) 448–455.
[29] R. Liang, W. Zong, S. Palcsey, S. Abramowitch, P.A. Moalli, Impact of prolapse meshes on the metabolism of vaginal extracellular matrix in rhesus macaque, Am. J. Obstet. Gynecol. 212 (2) (2015) 174, e1–174.e7.
[30] U. Klinge, B. Klosterhalfen, Modified classification of surgical meshes for hernia repair based on the analyses of 1,000 explanted meshes, Hernia 16 (3) (2012) 251–258.
[31] Zahrina Mardina, Jeffrey Venezuela, Christopher Maher, Zhiming Shi, Matthew S. Dargusch, Andrej Atrensb, Design, mechanical and degradation requirements of biodegradable metal mesh for pelvic floor reconstruction, Biomater. Sci. (2022), https://doi.org/10.1039/D2BM00179A.
[32] L.M. Zhu, P. Schuster, U. Klinge, Mesh implants: an overview of crucial mesh parameters, World J. Gastrointest. Surg. 7 (10) (2015) 226–236.
[33] L. Hympánová, R. Rynkevic, S. Román, M.G.M.C. Mori da Cunha, E. Mazza, M. Zündel, I. Urbánková, M.R. Gallego, J. Vange, G. Callewaert, C. Chapple, S. MacNeil, J. Deprest, Assessment of electrospun and ultra-lightweight polypropylene meshes in the sheep model for vaginal surgery, Jan 15, Eur. Urol. Focus 6 (1) (2020) 190–198, https://doi.org/10.1016/j.euf.2018.07.024.
[34] N. Sindhwani, Z. Liaquat, I. Urbankova, G. Vande Velde, A. Feola, J. Deprest, Immediate postoperative changes in synthetic meshes - In vivo measurements, J. Mech. Behav. Biomed. Mater. (2015) 228–235.